

Article

Pulse Magnetic Fields Induced Drug Release from Gold Coated Magnetic Nanoparticle Decorated Liposomes

Basanta Acharya and Viktor Chikan * 

Department of Chemistry, Kansas State University, Manhattan, KS 66506, USA; bacharya@ksu.edu

* Correspondence: vchikan@ksu.edu; Tel.: +1-785-532-6807

Received: 27 July 2020; Accepted: 13 October 2020; Published: 19 October 2020



Abstract: Magnetic nanoparticle-assisted drug release from liposomes is an important way to enhance the functionality/usefulness of liposomes. This work demonstrates an approach how to integrate magnetic nanoparticles with liposomes with the assistance of gold–thiol chemistry. The gold coated magnetic particles cover the thiolated liposomes from the outside, which removes the competition of the drug molecules and the triggering magnetic particles to free the inner space of the liposomes when compared to previous magneto liposome formulations. The liposome consists of dipalmitoyl phosphatidylcholine (DPPC) combined with distearoylphosphatidylcholine (DSPC) in addition to regular cholesterol or cholesterol-PEG-SH. Permeability assays and electron microscopy images show efficient coupling between the liposomes and nanoparticles in the presence of thiol groups without compromising the functionality of the liposomes. The nanoparticles such as gold nanoparticles, gold coated iron oxide nanoparticles and bare iron oxide nanoparticles are added following the model drug encapsulation. The efficient coupling between the gold coated nanoparticles (NPs) and the thiolate liposomes is evidenced by the shift in transition temperature of the thiolated liposomes. The addition of magnetically triggerable nanoparticles externally makes the entire interior of liposomes available for drug loading. The drug release efficiencies of these liposomes/NPs complexes were compared under exposure to pulsed magnetic fields. The results indicate up to 20% of the drug can be released in short time, which is comparable in efficiency to previous studies performed when magnetic NPs were located inside liposomes. Interestingly, the liposomes were found to exhibit variations in release efficiency based on different dilution media which is attributed to an osmotic pressure effect on liposomal stability.

Keywords: magnetic nanoparticles; pulsed magnetic field; ultrasound; liposomes; drug release; gold coated magnetic nanoparticles

1. Introduction

Liposomes are widely established, clinically approved, nano-sized lipid vesicles used as drug delivery agents [1,2]. They are flexible in size and composition [3], biocompatible, suitable for both hydrophilic and hydrophobic drugs and more stable than other lipid vesicles, which makes them applicable in biomedical research fields [1–5]. The advantage of liposomes over other lipid vesicles lies in their ability to load hydrophilic molecules in their aqueous cores [6,7] and hydrophobic ones in their bilayers [5,8]. In addition, the hydrophilic molecules dissolved in a liposome's aqueous core cannot easily pass through the bilayer, making it an efficient drug carrier [5–8]. The drug carrier is expected to be released from the liposome via passive or active stimuli [8–10]. There are a number of active stimuli that have been employed, such as change in temperature [9,11,12], magnetic field [10], pH [12,13], light [14], ultrasound [15] and radio-frequency [16] to trigger liposomes.

Through the incorporation of magnetic nanoparticles (MNPs), such as iron-oxide nanoparticles (IONPs), a new dimension has been added to the drug release process, allowing remote control via magnetic fields [10]. The MNPs in most cases, are encapsulated in an aqueous core along with drug molecules and then the entire system of MNP-loaded liposomes is exposed to an alternating magnetic field (AMF) [17,18], which triggers the release of drugs loaded in the liposomes by the process of magnetic hyperthermia [19]. MNPs like IONPs under an action of an AMF generate heat which results in an increase of temperature of the liposomes above the transition temperatures (T_m) of the constituent lipids [11,17,19]. This thermal disruption of the lipid bilayer releases the payload at the desired site and the excess heat serves in the thermal ablation to eliminate unhealthy tissues [10,11,17,19,20]. The challenge is that the magnetic hyperthermia triggered delivery is slow in relation to some important physiological processes (blood circulation) or to the lifetime of some thermo-sensitive drug molecules. Faster triggering could benefit this field by expanding the applications of liposomal drug delivery systems. Considering liposome preparation, the lipid composition can be chosen so that its transition temperature is near to 37 °C (normal human body temperature), but it may lead to the leakage of drug prior to reaching its target site. On the other hand, if the transition temperature of the liposome is higher than body temperature, then the release is slow and inefficient [4,10,11,19]. The requirement of using strong, continuous, high-frequency magnetic fields makes this approach challenging in the biomedical field [20–22].

Ultrasonically induced drug release provides a faster drug release mechanism in the case of liposomal drug delivery systems [23]. Many studies focusing on ultrasound triggering have shown that pressure waves involved in ultrasound disrupt the lipid bilayer mechanically, thereby increasing liposomal permeability, which leads to drug release [23,24]. This methodology is non-invasive, and ultrasound has a reasonable penetration depth of soft tissue, making it a powerful tool for triggered drug release [25]. Studies have revealed that low frequency ultrasound imparts only the mechanical effect, which is connected with cavitation, while high frequency ultrasound can induce both thermal and mechanical effects [23–25]. To elevate the system at appropriate temperature, high frequency ultrasound requires very high intensity of ultrasound power (1–100 W/cm²) that may not only impact liposomal drug delivery vehicles, but healthy tissue as well [23,25].

Colloidal magnetic nanoparticles can emit ultrasonic waves in the presence of high-frequency inhomogeneous magnetic fields [26]. The use of magnetic nanoparticles as sonosensitizers for the ultrasound generation has significantly enhanced its effectiveness for sonodynamic applications [26–28], due to the high penetration depths of inhomogeneous magnetic fields compared to that of ultrasound. In effect, the combination of a magnetic field and the use magnetic nanoparticles allows spatial focusing by concentrating the ultrasound at nanoscale. In case of liposomal drug delivery systems, mechanical disruption of lipid bilayer of liposomes via pulsed magnetic field-generated ultrasound has been proven effective for rapid (microseconds and milliseconds) and controlled release over traditional thermal (seconds and minutes) disruption of the bilayer of the liposomes. Ultrasound generation from magnetic NPs in inhomogeneous magnetic fields is more effective than ultrasound generated from magnetic NPs in homogeneous magnetic fields due to the so called magnetostriction effect [28–30]. Please, note that diamagnetic materials (liposomes, water, drugs) also respond to magnetic fields, but to a lesser extent so the use and location of magnetic nanoparticles is critical to magnifying the impact of the mechanical waves in biological applications.

In the previous works [8,17–19,31], the magnetic nanoparticles were loaded inside (either at core or within the bilayer) the liposomal drug delivery systems. This approach provides a fairly simple and robust way to combine the drug and the trigger. A fundamental drawback of this approach that there is a competition between drug and the triggering nanoparticles (NPs) for the space inside the liposome. The present work has two important novelties to enhance the efficiency of drug release. First, the magnetic nanoparticles have been moved outside the liposomes in their vicinity by using a chemical linker (Figure 1A; the chemical linker used here is a PEGylated cholesterol with one end modified with a thiol (-SH) group) instead of encapsulating them at the aqueous cores of liposomes or in

the bilayers of the respective liposomes. The relocation of the triggering particles provides more volume for drug encapsulation and the lack of competition between drug molecules and MNPs increases the drug release efficiency. A second less obvious advantage is that the drug release efficiency/trigger will be larger for a typical liposome (≈ 200 nm in diameter). Based on geometric factors, with calculations one can show that the theoretical drug release would be higher/NP for a typical liposome, drug, NP formulation (200 nm, 1 nm, 20 nm), as shown in Figure 1B. In order to provide a stable interaction of the liposome and magnetic NPs, a thin gold coating is applied on the iron oxide nanoparticles which adds the versatility of magneto-liposomes. Here, iron oxide NPs are used as the source for ultrasound generation on exposure to pulsed magnetic field while a gold coating provides efficient linking with the thiol ($-SH$) group present in the liposomal surface as sulfur–gold bond enthalpy is approximately 200 KJ/mol [32].

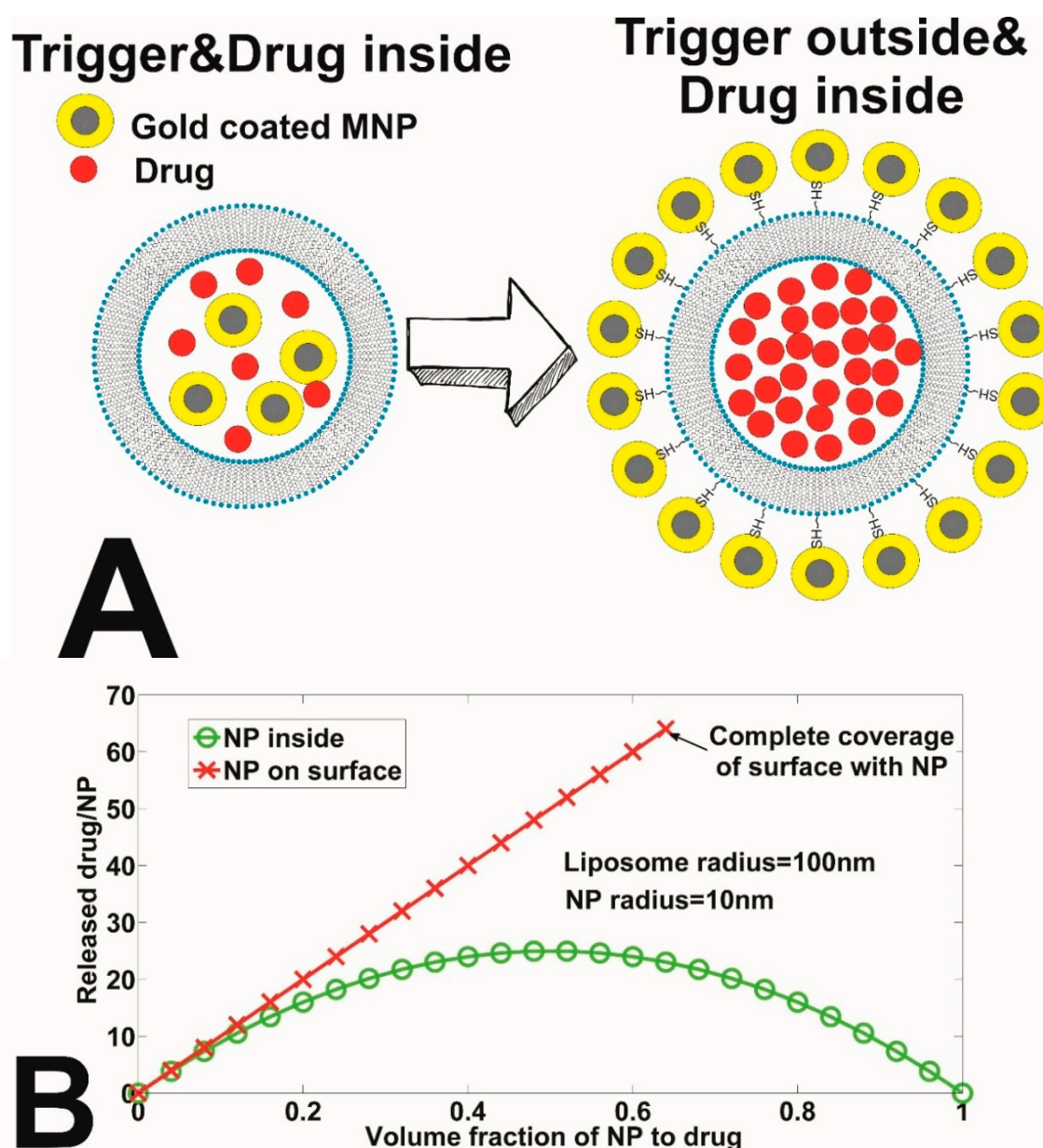


Figure 1. (A) Cholesterol–PEG–SH ligands to link nanoparticles with liposomes. (B) Calculated drug delivery efficiency as a fraction of Nanoparticle (NP) to drug for the two different compositions shown in (A). In this calculation, the triggering magnetic NP is assumed to be 10 nm in radius and the liposome as a radius of 100 nm.

The Role of Magnetic Field Duration in Triggering Magnetic Fields in Magneto-Liposome Experiments

In the past few decades, several magneto liposome formulations and experimental approaches have been used, which makes comparison of these experiments difficult from the basic physical chemistry standpoint. Table 1 provides a comparison of the various experimental data from the literature. In order to provide a new prospective on existing data of magneto liposome experiments, the drug release efficiencies were normalized to the duration of magnetic fields used. First, one can define the duty cycle of the magnet which will serve as a normalization factor for the Table 1. A duty cycle D is a fraction of a period during which a signal remains active and it is mathematically expressed in percentage or a ratio by

$$D = \frac{\text{Pulse Width (PW)}}{\text{Total period of signal (T)}} * 100\% \quad (1)$$

Table 1. Comparison normalized efficiencies of magneto liposomal drug delivery systems from literature. The data show that pulsed magnetic field induced drug release is more effective than other techniques when the unit time release is concerned.

Ref	Liposome/NP Formulation	Location of Trigger	Max Release (%)	Application Time (min)	Duty Cycle of Magnet (%)	Intensity of the Magnetic Field (mT)	Unit Time Release (% Release/s)
[8]	PC/CoFe ₂ O ₄	Bilayer	90	50	100	330	0.03
[10]	DSPC/PEG/IONPs	Bilayer	180	30	100	-	0.1
[19]	MPPC/SPION	Bilayer	90	6	100	94.5	0.25
[18]	HSPC/Fe ₃ O ₄	Core	20	180	9.77	1.5	0.00185
[31]	DPPC/FePt	Core	8.4	3.3 × 10 ⁻⁵	0.001	3000	248,000

In magnetic pulses applications, D varies from lower values (<1%) in pulsed magnetic fields to as high as 100% for alternating current (AC) magnetic fields (MF). The key reason is purely technological, which makes it easily produce transient intense magnetic fields or lower amplitude continuous magnetic fields. Alternating current magnetic fields (AC-MF) typically have 100% duty cycles, whereas in a pulsed magnetic field, pulses are triggered in an interval of a few seconds and the time of each pulse oscillation is in the microsecond range. In this work, magnetic pulses are triggered in an interval of 20 s and each pulse has 200 μs oscillation time which gives a 0.001% duty cycle, becoming 10,000 times more efficient than normal AC-MF. Since the time of application in pulsed MF is in order of microseconds compared to minutes in AC-MF hyperthermia processes, pulsed MF is far more advantageous than AC-MF. In addition, the field intensity in pulsed MF is in Teslas compared to milliTesla scale in AC-MF.

2. Results

2.1. Characterizations of Nanoparticles

Elemental analysis of samples of nanoparticles shows that the synthesized iron oxide nanoparticles (Table 2) have a percentage ratio of atoms Fe:O equal to 1:1.64 which is nearly 1.5. That suggests the particles formed are possibly Fe₂O₃ nanoparticles. However, the EDX alone cannot confirm the formation of Fe₂O₃. Based on the procedure discussed in methods section, the particles are further oxidized so they can also be Fe₃O₄. Nevertheless, the particles are the iron oxide, as revealed by EDX data. The presence of carbon in Table 2 and a carbon peak in Figure S2 (see the supporting information), is due to the tetramethyl ammonium hydroxide (TMAOH) used as a suspension medium for synthesized iron oxide nanoparticles.

Table 2. Elemental analysis of synthesized iron oxide nanoparticles.

Element	Weight %	Atomic %	Uncertainty %	Detector Correction
C	77.87	90.10	1.32	0.28
O	7.08	6.15	0.33	0.51
Fe	15.04	3.74	0.33	0.99

The elemental analysis of gold coated samples in Tables 3 and 4 show that the gold coating on commercial iron oxide nanoparticles have smaller Au ratios to gold coated on synthesized iron oxide nanoparticles. The lesser the ratio of gold, the lesser the dead mass for a magnetic particle. This is supported by the percentage release data shown in Tables 5 and 6, which clearly reveals that gold coated commercial iron oxide samples are more efficient at carboxy-fluorescein (CF) release. The EDX spectrum images of different types of nanoparticles are included in supporting information (see Figures S2–S6).

Table 3. Elemental analysis of gold coated synthetic iron oxide nanoparticles.

Element	Weight %	Atomic %	Uncertainty %	Detector Correction
O	22.60	76.61	2.73	0.51
Fe	2.98	2.89	1.38	0.99
Au	74.41	20.48	5.78	0.99

Table 4. Elemental analysis of gold coated commercial iron oxide nanoparticles.

Element	Weight %	Atomic %	Uncertainty %	Detector Correction
O	23.36	75.79	1.10	0.51
Fe	6.02	5.59	0.50	0.99
Au	70.60	18.60	2.40	0.99

Table 5. Percentage release of CF on interaction of regular liposomes with different nanoparticles under a pulsed magnetic field.

Volumes of NPs (μ L)	Commercial Iron Oxide NPs	Gold coated Commercial IONPs	Synthetic Iron Oxide	Gold Coated Synthetic IONPs
0	5.5%	5.2%	5.0%	5.4%
2	2.1%	3.4%	5.8%	2.7%
4	2.6%	10.8%	2.9%	3.0%
6	1.2%	9.8%	2.5%	5.8%
8	1.3%	9.3%	3.7%	2.8%
10	0.9%	6.3%	4.0%	3.6%

Table 6. Percentage release of CF on interaction of 50% Thiolated Cholesterol (Th-Chol) liposomes with different nanoparticles under pulsed magnetic field.

Volumes of NPs (μ L)	Commercial Iron Oxide NPs	Gold coated Commercial IO NPs	Synthetic Iron Oxide	Gold Coated Synthetic IO NPs
0	4.8%	4.5%	4.7%	4.6%
2	5.0%	7.5%	10.5%	6.5%
4	3.6%	14.2%	6.6%	7.5%
6	9.5%	17.6%	7.5%	9.9%
8	3.9%	20.5%	5.6%	7.6%
10	3.8%	14.6%	7.4%	6.8%

The transmission electron microscopy (TEM) images of the nanoparticles used in this work are shown in Figure 2. Figure 2A has TEM images for commercial iron oxide nanoparticles (Fe_3O_4)

obtained from the website of US Research Nanomaterials Inc. The size of the particles is between 15 and 20 nm as mentioned on the website of the manufacturer. Figure 2B shows the distribution of synthetic iron oxide nanoparticles. Figure 2C,D represents the gold coated samples for commercial and synthesized iron oxide nanoparticles, respectively. The TEM images show the homogeneity and uniformity in size of “in-house made” nanoparticles.

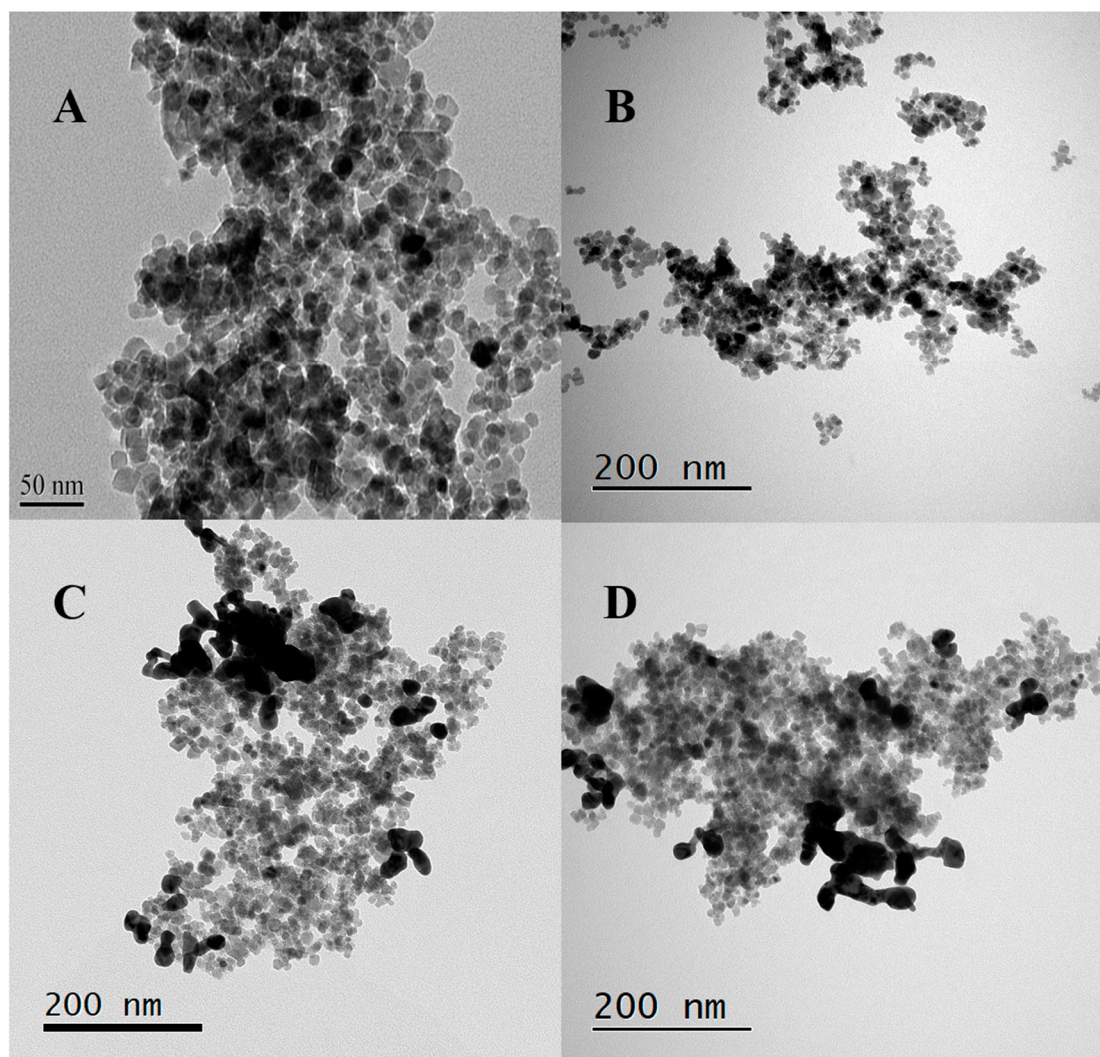


Figure 2. TEM images. (A) Commercial iron oxide nanoparticles (image from www.usnano.com). (B) Synthetic iron oxide nanoparticles. (C) Gold coated commercial iron oxide nanoparticles (D). Gold coated synthetic iron oxide nanoparticles. (See the supporting information in Figure S1A–C for more TEM images).

2.2. Characterization of Liposomes—Nanoparticle Composites

The TEM images (Figure 3), provide evidence for the interaction between thiolated liposomes and gold coated iron oxide nanoparticles. The images in Figure 3 show that thiolated liposomes have greater affinity towards the gold coated magnetic nanoparticles compared to the regular liposomes without thiol groups. The concentration of nanoparticles at the interface of liposomes, in Figure 3A–C, strongly indicates that the proposed formulation of magneto-liposomes was accomplished. In Figure 3D the lesser nanoparticles around the liposomes are as per our expectation because the regular liposomes lack thiol groups to bind the gold coated MNPs. The negative staining method was used for TEM images (see the supporting information for the detailed procedure of the negative staining method).

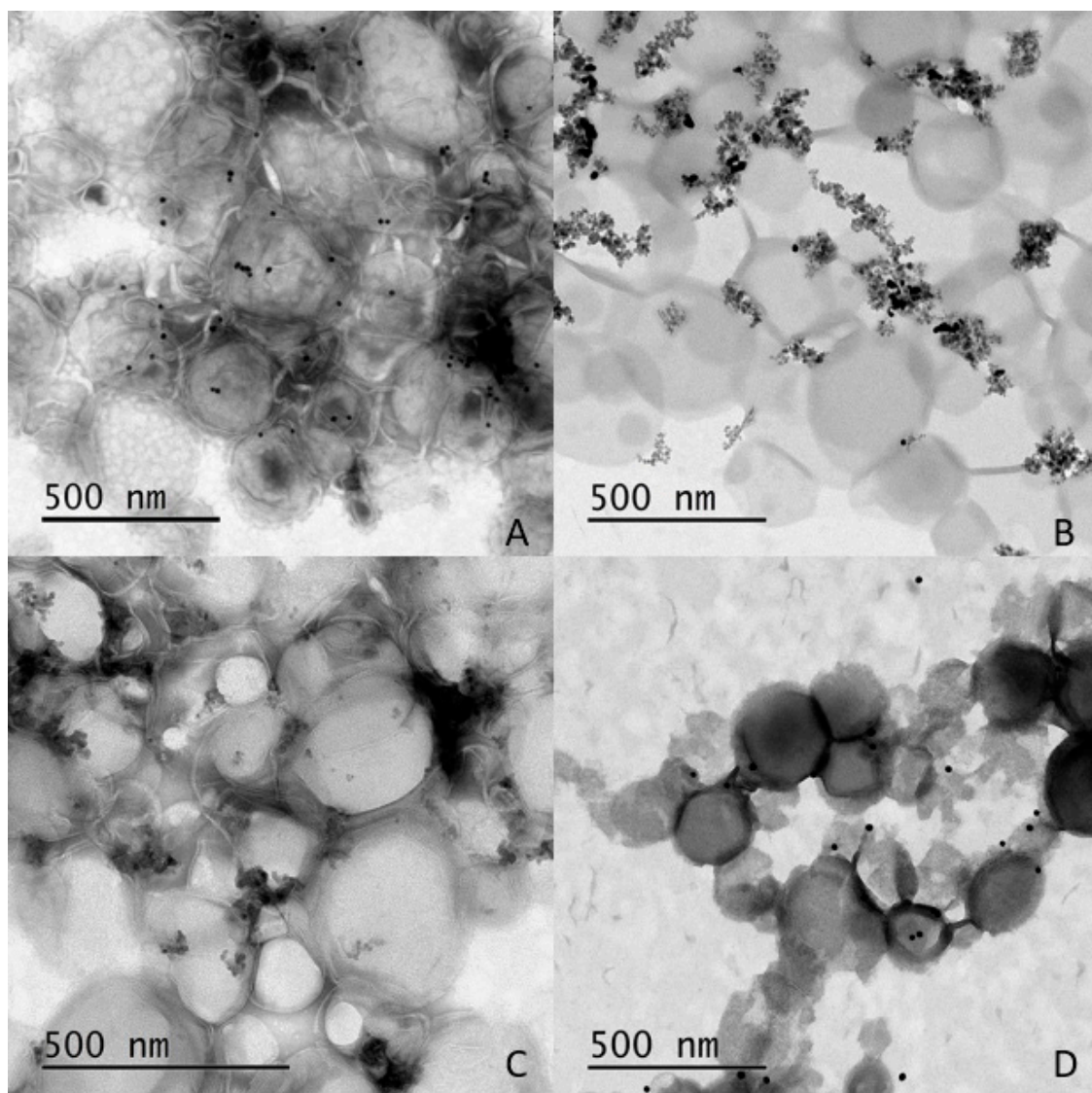


Figure 3. TEM images. (A,B) Thiolated liposomes with gold coated synthetic iron oxide NPs. (C) Thiolated liposomes with gold coated commercial iron oxide NPs. (D) Regular liposomes with gold coated commercial iron oxide NPs. (See the supplementary materials, Figure S7, for the rest of the images that exhibit the chemisorption of gold coated MNPs on the liposomal surface by gold–thiol bonds).

2.3. Changes in the Transition Temperature of the Liposomes upon Addition of Nanoparticles

Two different types of liposome samples (regular liposomes with no thiol groups and thiolated liposomes with 50% Th-CHOL) are allowed to interact with different types of nanoparticles. The percentage photoluminescence (PL) intensity vs. temperature graphs (Figure 4A,B) show that addition of nanoparticles results in a change of transition temperature of liposomes. For the regular liposomes without thiol groups (Figure 4A), the change in transition temperature (with reference to a sample without nanoparticles) is negligibly small upon addition of the iron oxide NPs and gold nanoparticles (AuNPs 40 nm size), while there is small change (decrease by approximately 3 °C) when interacting with 50 nm in size gold coated iron oxide NPs. These indicate that there is no significant interaction between the liposomes and nanoparticles. However, for the thiolated sample (Th-Chol 50%) in Figure 4B, the interaction with nanoparticles is such that the transition temperature changes by 3 to 8 °C.

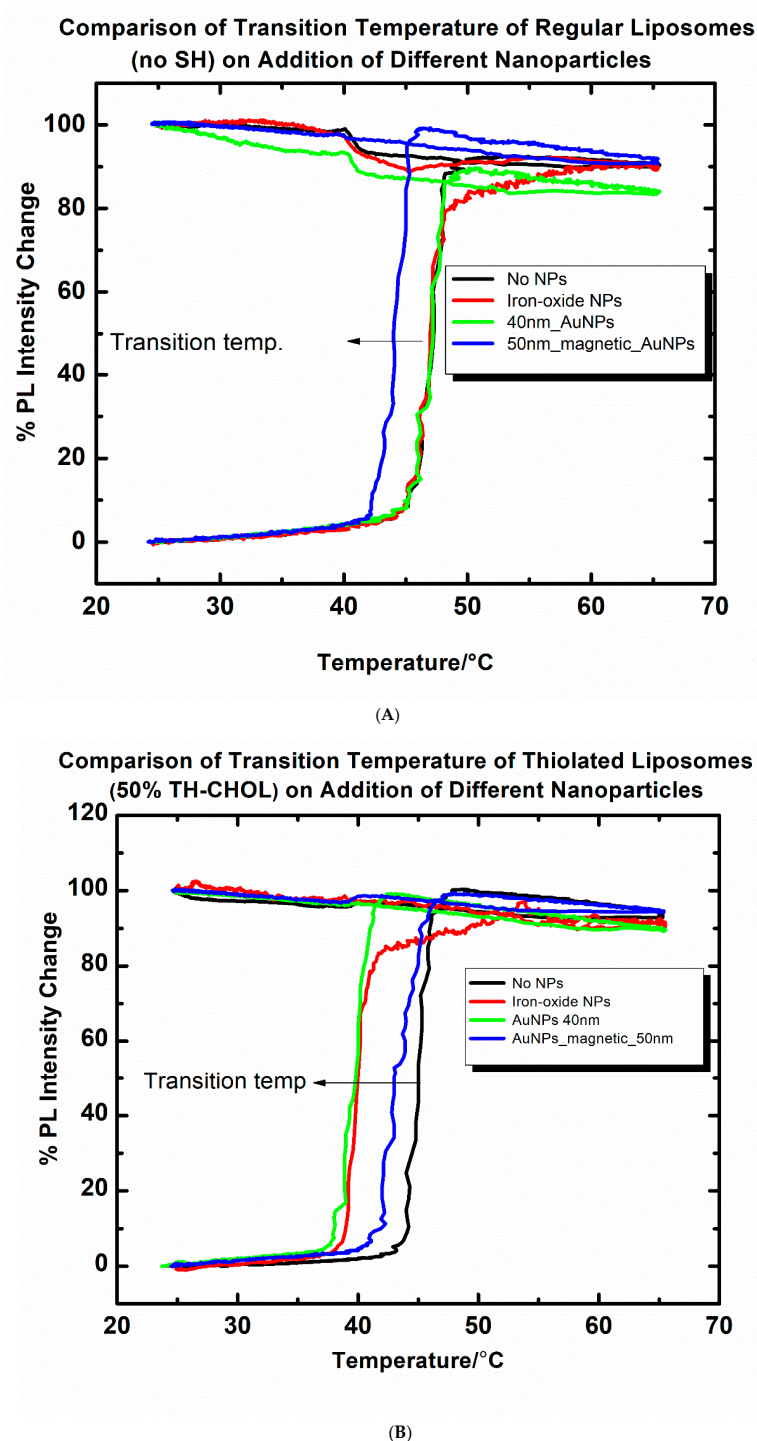


Figure 4. (A) Comparison of transition temperatures of regular (non thiolated) liposomes with various nanoparticles (see text for detail). Please, note that the PL intensity is normalized to 0–100% at 25 °C for comparison. (B) Comparison of transition temperatures of thiolated (with 50% Thiolated cholesterol) liposomes with various nanoparticles (see text for detail). Please, note that the PL intensity is normalized to 0–100% at 25 °C for comparison.

The data show that the formation of the liposome/NP complexes takes place on a relatively slow timescale. To investigate the kinetics of interactions of magnetic Au NPs (50 nm) with regular and thiolated liposome samples, a separate experiment was carried out. In Figure 5A,B the data show that when magnetic AuNPs interact with liposomes, interaction is evidenced by the change in

transition temperature. The transition temperature exhibits the time-dependence of this interaction and varies with the liposome composition. For the regular liposome sample, the change in transition temperature seems to be over in a relatively short amount of time (5 min) and for the Th-Chol 50% sample, the transition temperature continues to shift lower over longer periods of time. In addition, the absolute value of transition temperature change is larger than in the case of regular liposomes. Please, note that the slow kinetics can be observed since the heating curve takes about an hour to obtain in this particular experimental setup.

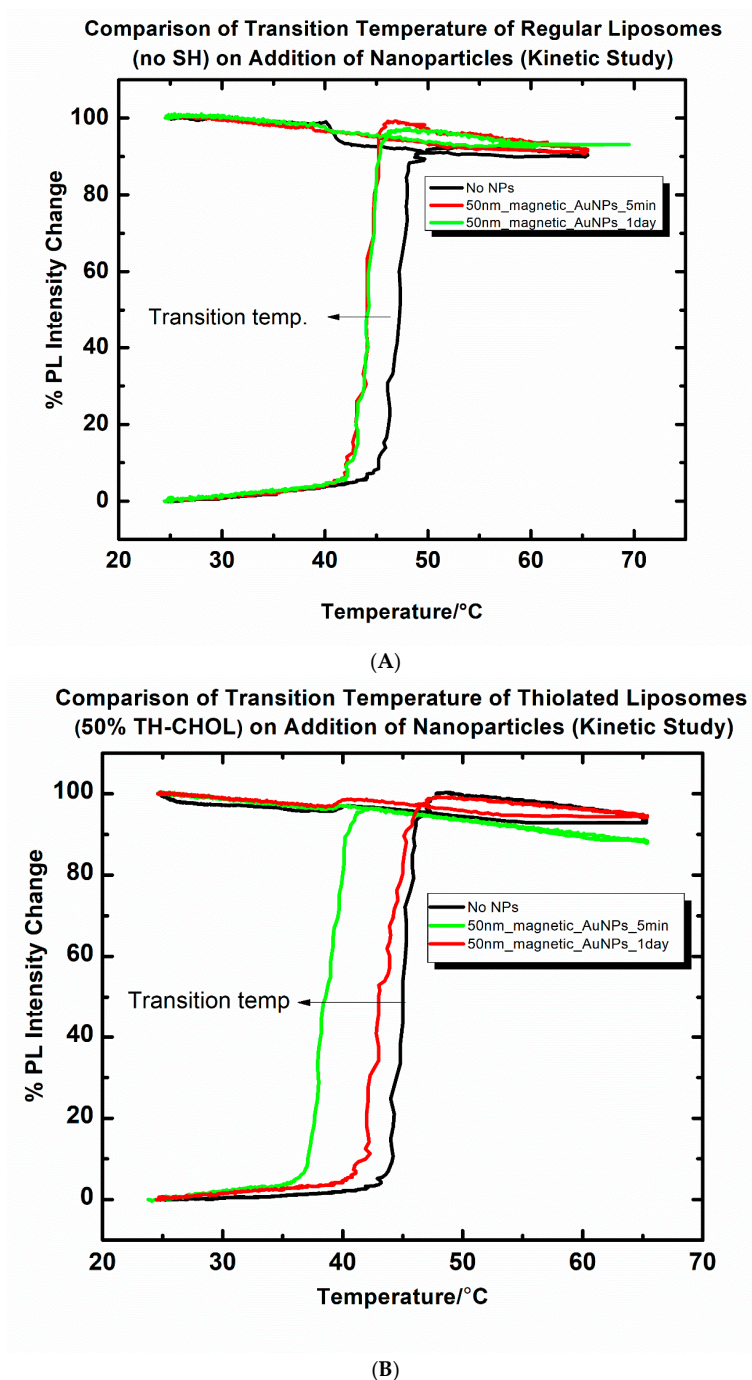
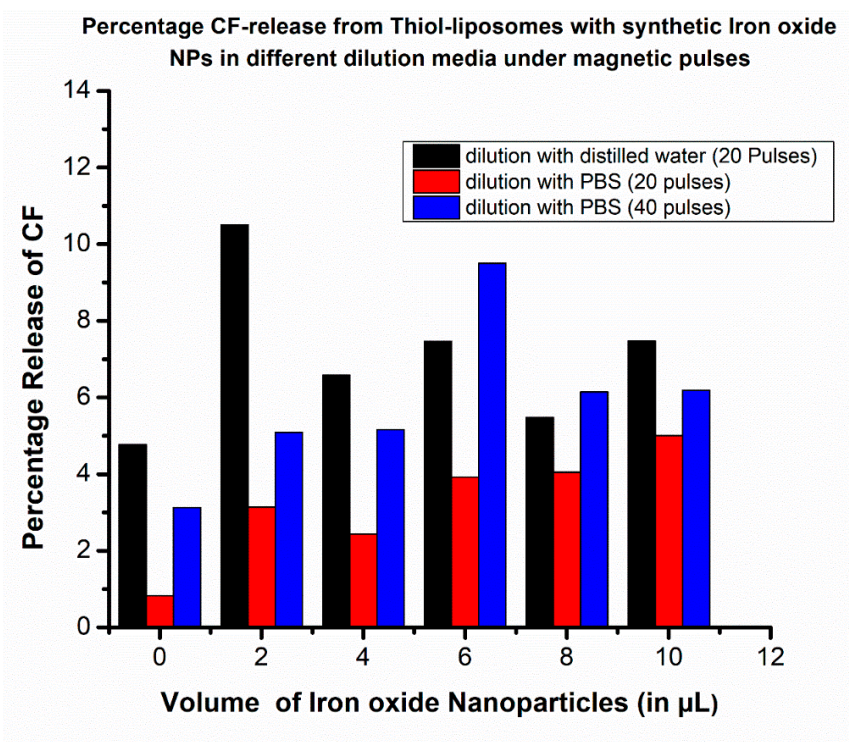


Figure 5. (A) Kinetics of interactions of 50 nm magnetic AuNPs with regular liposomes. (B) Kinetics of interactions of 50 nm magnetic AuNPs with thiolated liposomes (Th-Chol 50%).

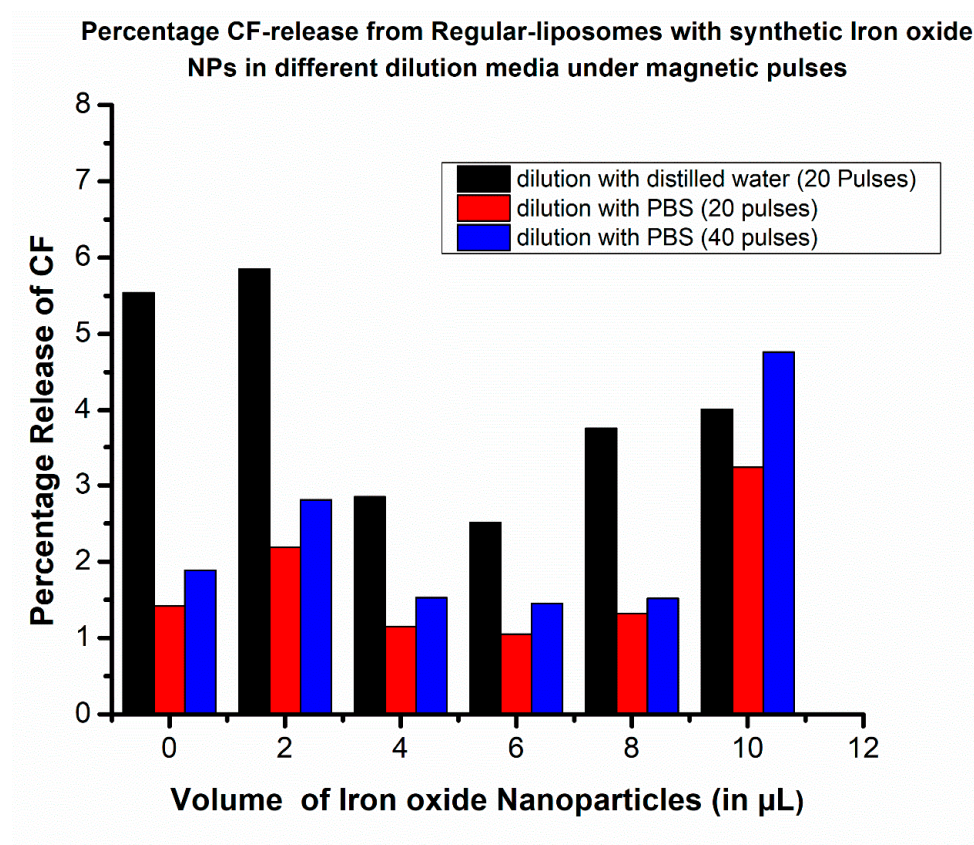
2.4. Pulsed Magnetic Field Triggered Drug Release from MNP-Coated Liposomes: The Impact of Dilution (Osmotic Pressure)

Osmotic pressure can build up if the chemical potentials of the solvent are different on the two sides of a membrane. One might anticipate that osmotic pressure may have significant impact on the liposomal stability. The build up from the osmotic pressure could also lead to “pressure priming” the liposomes to accelerate drug release upon triggering. We investigated the release of CF from thiolated and regular liposomes combined with synthetic iron oxide nanoparticles under the pulsed magnetic field under various dilution conditions. For this, two different dilution media, distilled water and 1× PBS (phosphate buffered saline), were used. Dilution of liposome samples would result in larger osmotic pressure in the case of distilled water. In order to minimize the impact of the gold–thiol bond interaction under different dilution conditions, bare iron oxide MNPs were chosen. The concentration of the iron oxide nanoparticle solution was 170 g/L, and the iron oxide nanoparticles were added to a 2 mL diluted solution of liposomes, and after 5 min, the release study was carried out. The data are presented in Figure 6A,B exhibiting the release of CF dye under different conditions and with increasing numbers of pulses. The graph in Figure 6A shows that the thiolated liposomes diluted with water as dilution media exhibit a higher percentage of release of CF dye compared to PBS as dilution medium, under same number of magnetic pulses (20 pulses) in the whole series of different volumes of nanoparticles used. Even the 40 magnetic pulses in PBS dilution media have lower release than with 20 pulses in water media (except in 6 and 8 μ L). The graph in Figure 6B shows similar studies for the regular liposomes with different dilution media under magnetic pulses. The release percentage is almost double when liposomes are diluted in distilled water as compared to dilution in a 1× PBS solution. In conclusion, while liposomal drug delivery systems utilize buffers to stabilize the liposomes, dilution will impact the drug release efficiency and the stability of the liposomes. Even the liposomes that have no NPs show noticeable release after applications of 20 magnetic pulses; therefore, in the next step the experiments were carried out in distilled water as dilution media.



(A)

Figure 6. Cont.



(B)

Figure 6. (A) Effect of dilution media on the thiolated liposome-iron oxide NP system under a pulsed magnet. (B) Effect of dilution media on the regular liposome-iron oxide NP system under a pulsed magnet.

2.5. Pulsed Magnetic Field Triggered Drug Release from MNP-Coated Liposomes: Comparison of Adding Thiolated and Non-Thiolated Liposomes

The goal of utilizing gold coated magnetic particles and covering the surfaces of liposomes with $-\text{SH}$ bonds is to localize ultrasound close to the lipid membrane for an effective drug delivery system. In this study, we investigated the percentage release of carboxyfluorescein liposome/NP complexes consisting of the regular and thiolated phospholipids under the pulsed magnetic fields. The types of magnetic nanoparticles used in the experiments were: commercial iron oxide NPs, gold coated commercial iron oxide NPs, synthetic iron oxide NPs and gold coated synthetic iron oxide NPs. All the nanoparticle solutions were normalized to the concentration of commercial iron oxide nanoparticles (170 g/L) and the nanoparticle solution was added at different volumes in each experiment ranging from 0 to 10 μL onto the liposome samples (2 mL). The results of percentage release of CF dye for regular and thiolated liposomes with distilled water as dilution media are summarized in Tables 5 and 6. As shown in the data, the release efficiencies after application of 20 magnetic pulses varied from 1% to 20%. Overall, the gold coated commercial iron oxide particles combined with thiolated liposomes exhibited the best drug release efficiencies.

3. Discussions

3.1. Effect of Nanoparticles on Liposomal Transition Temperature

In the previous works [8,17–19,33], the magnetic nanoparticles were loaded either at the hydrophilic cores or at the lipid bilayers of liposomes. Hydrophilic MNPs disperse in the aqueous core,

whereas hydrophobic MNPs can interact with bilayers. These binding interactions are mainly electrostatic; however, binding can take place under non-favorable electrostatic contributions that involve van der Waal forces [34]. It has been found that the incorporation of hydrophilic gold nanoparticles at the liposomal lipid bilayer results in membrane softening relative to pure liposomes, manifested by reducing bending modulus. The membrane softening phenomena is both size and concentration dependent [35]. Some investigations include perturbation of lipid properties upon nanoparticle adsorption, based on atomistic simulations. It has also been observed that nanoparticles penetrate shallowly into the bilayer, leading to local membrane thinning and bending [36].

In this work, the nanoparticles were added outside the liposomes where the interaction was based on physisorption in the case of regular liposomes. However, the interaction was based on chemisorption, in the case of thiolated liposomes. It is clear from the graph in Figure 4B that there is a change in transition temperature of liposomes only when the nanoparticles are added. Thus, it is the nanoparticles that cause some interaction with lipid bilayer resulting the shift in T_m . The type of interaction is yet to be explored in detail. Further, the kinetic studies (Figure 5A,B) for the interaction of nanoparticles and liposomes suggest that the interaction of thiol group with gold coated MNPs is time dependent. More experiments based on time-dependent interactions are required to explore the detailed mechanism.

3.2. Effect of Osmotic Pressure on Drug Release

As depicted by the graphs in Figure 6A,B the CF release is enhanced upon dilution with distilled water compared to the PBS mediated dilution, under a pulsed magnetic field. The overall increase in the release can be explained based on osmotic pressure effect on liposomal stability. The aqueous core of liposomes contained CF dye dissolved in PBS. When liposomes are diluted with distilled water, the concentration of ions is higher at the core compared to the surroundings of liposomes. Hence, osmotic behavior aids the liposomal bilayer disruption under magnetic pulse. However, dilution with PBS makes an isotonic environment at both the core and the surroundings so that the magnetic pulses solely contribute towards bilayer disruption; thus, the overall percentage release of the dye is lesser compared to the release under dilution with distilled water.

3.3. Comparative Drug (Cf) Release Study from Thiolated and Non-Thiolated Liposomes with MNP Coatings under a Pulsed Magnetic Field

The release of CF (4.5%–5.5%) was observed for both types of liposomes even in the absence of nanoparticles (i.e., 0 μ L in Tables 5 and 6). This is probably due to the diamagnetic behavior of water that assists the release under the high magnetic field of about 5 T and the distortion leading to leakage in the bilayer of the liposomes under these conditions [37–39]. Among the different types of nanoparticles employed, the gold coated commercial iron oxide nanoparticles provide greater release (as high as 20.5%) of CF dyes from thiolated liposomes and about 10.8% release from regular liposomes. This is potentially due to the bigger size (15–20 nm magnetic core) of these particles than the “in-house” synthesized nanoparticles samples (8–12 nm magnetic core). It is obvious that the bigger magnetic particles possess greater magnetic moments under application of a magnetic field, and hence ultrasound generation is more effective. In a similar study with cells [40], the iron oxide nanoparticles (25 nm diameter) were found to induce microporation within cells under pulsed magnetic field application. Thus, we anticipate that magnetic nanoparticles can trigger the drug release by the microporation of lipid bilayer of liposomes, triggered by pulsed magnetic field. Both commercial and synthetic iron oxide nanoparticles contribute release as high as 9.5–10.5% with thiolated liposomes, while with regular liposomes, release is limited to below 6%. The iron oxide nanoparticles still contribute to less overall release than gold coated samples, which is to be expected as these particles do not reside closer to liposomes. The gold coated synthetic iron oxide nanoparticles exhibit the release in the range of 5% to 10% depending on the volumes of nanoparticles added. From the results in Tables 5 and 6, it was revealed that gold coated nanoparticles contribute towards greater release than

bare iron oxide nanoparticles. This was expected, as gold coated samples tend to reside in the close vicinity of liposomes due to gold–thiol (Au–SH) bonds, which are absent in case of bare iron oxide nanoparticles. Additionally, the thiolated liposomes are more efficient towards release than simple, regular liposomes that lack thiol (-SH) groups.

4. Materials and Methods

The lipids and the regular cholesterol required for the liposome preparation were purchased from Avanti Polar Lipids (Alabaster, AL). Lipids used in the liposome preparation were (I) 1,2-dipalmitoyl-sn-glycero-3-phosphocholine (DPPC, MW = 734.05) and (II) 1,2-distearoyl-sn-glycero-3-phosphocholine (DSPC, MW = 790.16). Two different types of cholesterol were used in the experiments: regular cholesterol and cholesterol–PEG–SH. The latter was purchased from Nanocs Inc. (Fifth Avenue, New York, NY, USA). Other chemicals and gold nanoparticles (40 nm gold NPs and 50 nm magnetic gold NPs) were purchased from Sigma Aldrich). Commercial iron oxide NP (Fe_3O_4 , 99.5+%, 15–20 nm, 20% W in water) samples were purchased from US Research Nanomaterials Inc. (Houston, TX, USA). Syringes required for the extrusion of liposomes (1 mL, Model 1001 TLL SYR) were purchased from Hamilton Robotics (Reno, NV, USA). Polycarbonate filters (25 mm diameter, 0.2 μm pore size) were purchased from Spi Supplies (West Chester, PA, USA).

4.1. Preparation of Liposomes with Carboxyfluorescein (CF) Encapsulation

Liposomes were prepared by the thin film hydration method coupled with extrusion method in sequence, as described by Podaru et al. [31] Initially, chloroform solutions of lipids DPPC and DSPC were mixed together in a vial along with cholesterol in a molar ratio of 88:1:10 such that the total mixture of lipid was 10 mg. The chloroform was evaporated from the solution at 55 °C first, followed by vacuum evaporation for 1 h. The hydration of thin film of lipid was carried out by adding 1 mL of 1 \times PBS (phosphate buffered saline, prepared by dissolving 4 g of NaCl, 0.1 g of KCl, 0.72 g of Na_2HPO_4 and 0.12 g KH_2PO_4 in 500 mL of distilled water buffered to pH 7.4). The model drug 5(6)-carboxyfluorescein, a 100 mM solution of CF, was prepared in 1 \times PBS which was then titrated with 3M NaOH. For the CF loaded samples of liposomes, 1 mL of dark red solution of dye prepared in PBS was added to thin lipid film instead of pure PBS. After addition, the mixture was vortexed for 5 min to help creating multilamellar liposomes. The freeze/thaw process was then carried out where the vial containing sample was placed in a water bath (50 °C) for 5 min and then placed in dry ice for 5 min, repeatedly for 10 times such that at the end of the cycle, the solution remained in a hot water bath. The process called large unilamellar vesicles by extrusion (LUVET) was used in the next step, which produces unilamellar liposomes. The multilamellar liposomes at 50 °C were extruded through a 0.2 μm pore diameter polycarbonate filter 11 times, which yielded around 250 nm diameter liposomes, as verified with dynamic light scattering. Finally, non-entrapped free dye was separated by gel filtration chromatography using Sephadex G-50 size exclusion column. The liposomes were collected in the first fraction from the column. The dynamic light scattering measurements (Malvern Zeta-sizer Nano, Malvern Instruments, Malvern, UK) showed that the size of liposomes was about 200 nm (Figure S8 in supporting information shows the graph for size distribution of liposomes, obtained from DLS measurement. The average diameter of liposomes was 192.5 nm and polydispersity index, PDI, was 0.139).

4.2. Synthesis of Iron-Oxide Core/Gold Shell Nanoparticles

As shown in the literature, iron oxide nanoparticles synthesized in both organic [41,42] and aqueous medium [43] can be used as base material for creating gold coated NPs. However, the nanoparticles produced in organic phases require further conversion to aqueous phase via phase transfer reactions. The present magneto-liposome formulation requires water soluble nanoparticles which can be directly added to the aqueous surroundings of liposomes; therefore, iron oxide nanoparticles were synthesized in an aqueous phase followed by gold coating onto their surfaces at room temperature.

4.2.1. Method I: Gold Coating on Commercial Iron Oxide Nanoparticles

Hydroxyl amine hydrochloride ($\text{NH}_2\text{OH}\cdot\text{HCl}$), chloroauric acid trihydrate ($\text{HAuCl}_4\cdot 3\text{H}_2\text{O}$) and sodium citrate were purchased from Sigma Aldrich. The coating was carried out as described by Lyon et al. [43], with slight modifications. The reaction took place at room temperature by mixing reagents together. Commercial iron oxide NPs (Fe_3O_4 , 99.5+%, 15–20 nm, 20% W in water) were diluted to the concentration of 4.1675 g/L. For gold coating, the iron oxide NPs and sodium citrate solutions were taken in 2:1 volume ratio; i.e., 11.7 mL of diluted iron oxide NPs and 5.35 mL of 0.1 M sodium citrate solution were mixed. The mixture was diluted by adding 100 mL of water and stirred for 15 min. Then 535 μL of 0.2 M $\text{NH}_2\text{OH}\cdot\text{HCl}$ and 445 μL of 0.127 M $\text{HAuCl}_4\cdot 3\text{H}_2\text{O}$ were added and stirred. The color of the solution slowly changed to pink indicated the presence of reduced gold.

4.2.2. Method II: Gold Coating on Lab Synthesized Iron Oxide Nanoparticles

(A) Synthesis of iron oxide nanoparticles

Chemicals required for the synthesis, hexahydrate ferric chloride ($\text{FeCl}_3\cdot 6\text{H}_2\text{O}$), tetrahydrate ferrous chloride ($\text{FeCl}_2\cdot 4\text{H}_2\text{O}$), sodium hydroxide (NaOH), hydrochloric acid (HCl), nitric acid (HNO_3) and tetramethyl ammonium hydroxide (TMAOH) were purchased from Sigma Aldrich and used without further purifications. The Fe_3O_4 nanoparticles (cores) were prepared by coprecipitation of Fe (II) and Fe (III) chlorides (Fe(II)/Fe(III) ratio is 0.5) in an alkaline solution by the method of Lyon et al. [43] with minor modifications. Briefly, 4.595 g of Fe (III) chloride and 1.71 g of Fe (II) chloride were dissolved in 20 mL of distilled water in the presence of 100 mL of 2M HCl . The solution was then stirred vigorously until the Fe salts were dissolved. Subsequently, a solution of 2M NaOH was added dropwise into the mixture with vigorous stirring, resulting in a pale-yellow solution which changed to brown and finally to dark black. The black precipitate was collected on a 3000 Gauss permanent magnet, and washed twice with H_2O , once with 0.1M TMAOH then isolated via centrifugation. To obtain oxidized Fe_3O_4 nanoparticles, the precipitate (from above) was washed in 0.01 M HNO_3 . The particles were then dissolved in 0.01 M HNO_3 and heated at 65 °C with stirring until the color of the solution became brown. The oxidized Fe_3O_4 nanoparticles were suspended in 0.1M TMAOH after washing with water.

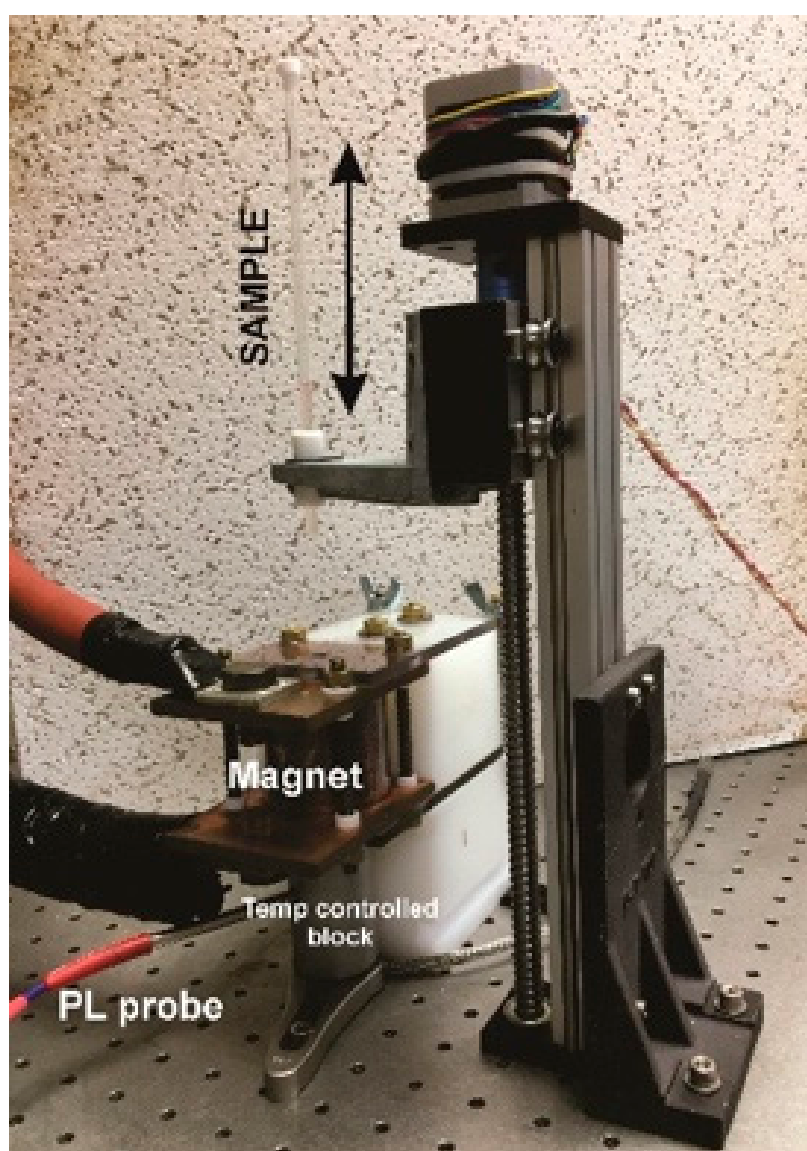
(B) Preparation of Au–Fe oxide composite nanoparticles

Au-shell coating was performed by reduction of Au^{3+} on the surface of Fe_3O_4 using a modification boiling citrate seeding procedure reported by Brown et al. [44]; 3 mL of the 0.212 mM $\text{N}(\text{CH}_3)_4$ -stabilized, oxidized Fe_3O_4 stock solution was diluted with 6 mL of 0.01 M sodium citrate and stirred for 30 min to exchange absorbed OH^- with citrate ions to make the final working magnetic-core solution; 1 mL of this solution was diluted with 3 mL of 0.01 M sodium citrate solution. The reaction solution containing magnetic cores and reduction agent was first sonicated for 15 min and then heated to 65 °C while vigorously stirring the solution. One milliliter of the solution of HAuCl_4 was added as soon as the solution reached 65 °C, and 15 min after the addition of Au^{3+} salts (10 mM solution of HAuCl_4), the heating was stopped, but stirring was continued till the solution cooled to room temperature. At this stage, a dark red/purple solution of gold coated iron oxide nanoparticles was obtained.

4.3. Description of Pulsed Magnetic Field for Ultrasound Generation

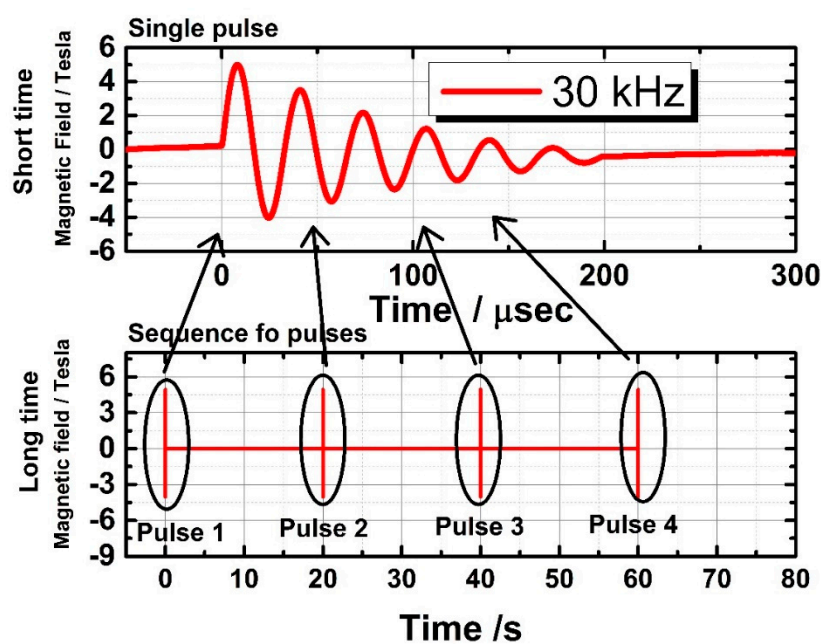
The pulsed magnetic field was generated as described in detail by Podaru et al. [28] Briefly, the inhomogeneous magnetic field was generated with the help of a pulsed power delivery system, which can produce 40,000 amps current in an external circuit in a short amount of time. The current source when turned on with the help of triggering switch, resulted in an oscillating current in the RLC circuit (circuit consisting of a resistor, an inductor, and a capacitor) producing approximately 200 μsec inhomogeneous magnetic pulses inside the anti-Helmholtz coil. Inside the coil, the off center measured peak magnetic field amplitude was approximately 5 Teslas. The magnetic pulses were

applied in an interval of 20 s which allowed recharging of the capacitor. The arrangement of a couple of coils in an anti-Helmholtz coil allows the production of opposing magnetic fields in each coil so that a large magnetic field gradient (~ 800 T/m) can be produced at the center of the coil, but zero magnetic field amplitude. This magnetic field gradient is responsible for creating translational motion of the iron oxide nanoparticles in the magneto liposomes, which results in generation of ultrasonic waves. The inhomogeneous magnetic field is preferred in the experiment, as the homogeneous magnetic field generating ultrasound via magnetostriction is less efficient. The magnet was integrated with an automatic sample handling system to lower the small amount of sample into the magnet and to then transfer the sample to a temperature-controlled metal block integrated with a fluorescence probe (Figure 7A). This automatic delivery system provided excellent repeatability in the experiments. This device allowed us to obtain photoluminescence (PL) measurements and expose the sample to inhomogeneous magnetic pulses with excellent reproducibility.

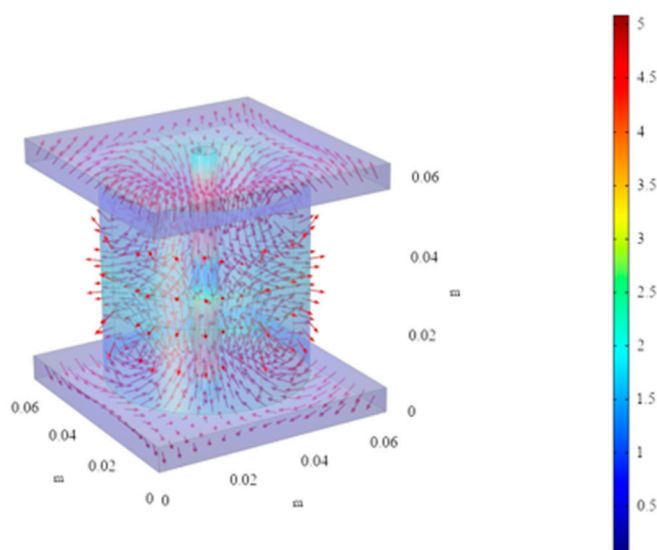


(A)

Figure 7. Cont.



(B)



(C)

Figure 7. (A) Integrated pulsed magnetic field and temperature dependent PL measurement system. For magnetic field exposure, the sample was lowered into a temperature-controlled metal block. PL was monitored with the help of Raman fluorescence probe. (B) The upper graph shows the magnetic pulse in one of the coils of the anti-Helmholtz coil pair and the graph below shows the sequence of the magnetic pulses as they are applied. (C) The magnetic vector field inside the coil modelled with COMSOL multiphysics software. The scale bar shows the intensity of the magnetic field in Teslas. The sample was placed in the center of this magnet where the magnetic field was zero, but the magnetic field gradient was large (~ 800 Tesla/m) The sample with small sample volume was placed in the center of the coil for the experiments.

4.4. Carboxyfluorescein Permeability Assay

The encapsulated carboxyfluorescein (CF) dye from the liposomal core was monitored by fluorescence measurement. When carboxyfluorescein is strongly packed inside the liposomes the fluorescence of this dye is self-quenched, resulting in little fluorescence. Once the dye has been released from the liposomes, its fluorescence strongly increases, which can be used to characterize the amount of drug released from liposomes. A fraction of liposome sample obtained from a column separation was diluted 10 times from the original (200 μL diluted to total volume of 2 mL), with distilled water (see supporting information for the concentration of liposomes per sample). In the next step, magnetic nanoparticles were added to the diluted liposome solution. Then 200 μL of sample were taken in an NMR tube and kept in a cylindrical hollow loop, as shown in a Figure 7A above. The delay stage helps to raise and lower the sample tube as needed and controlled by a LabVIEW software written for this purpose. Initially, the background fluorescence of sample was measured, before applying magnetic pulses. The sample tube was then raised to the center of anti-Helmholtz coils where the magnetic field gradient was maximal. Exactly 20 pulses were applied on the sample and sample was then lowered to measure the fluorescence. After measuring post magnetic pulse fluorescence, the sample was subjected to a thermal cycle, where temperature gradually increased at the rate of 0.1 $^{\circ}\text{C}/10$ s, with the help of metal jacket connected to the temperature controller. Fluorescence data were recorded after the completion of a thermal cycle (increased from initial 25 $^{\circ}\text{C}$ to 65 $^{\circ}\text{C}$ and cooled back to 25 $^{\circ}\text{C}$). Liposomes were fully lysed when heated to 65 $^{\circ}\text{C}$, thereby releasing all the dyes enclosed at the core. Figures S9 and S10 in the supporting information show that all the samples have fairly comparable CF encapsulation and release. This provides strong evidence of reproducibility of the CF permeability assay described here. The CF release is measured as a factor of

$$\text{Release factor of CF (f}_{\text{max}}) = \frac{\text{total fluorescence after thermal cycle}}{\text{initial background fluorescence}} \quad (2)$$

For photoluminescence intensity percentage change,

$$\% \text{PL intensity change} = 100 \frac{f_{\text{d}}/f_{\text{i}} - 1}{f_{\text{max}} - 1} \quad (3)$$

where,

f_{d} = fluorescence data points;

f_{i} = initial background fluorescence data point;

f_{max} = maximum value of fluorescence release factor;

1st fluorescence data point/initial background fluorescence = 1 (normalized).

Once the % PL intensity change is measured at each temperature from 25 $^{\circ}\text{C}$ to 65 $^{\circ}\text{C}$ range, a plot for CF permeability assay looks like figure below (Figure 8).

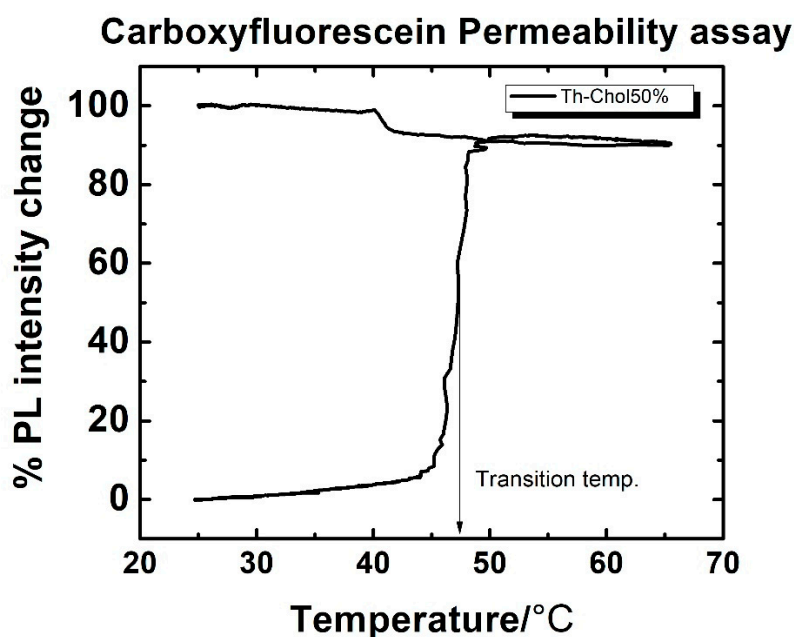


Figure 8. Typical PL curve of the liposomes loaded with CF. The PL slowly increases with temperature as the CF starts leaking out from the liposomes. When the temperature reaches the transition temperature of the liposomes, it releases its load. When the heated sample undergoes cooling, the PL will gradually increase till room temperature reached again. The initial and final PL provide the measuring stick for the amount of drug released from the liposomes!

5. Conclusions

The change in transition temperature of liposomes in presence of nanoparticles indicates interaction of the liposomes with gold coated magnetic nanoparticles. In addition, it has been found that thiolated liposomes show greater interaction, as compared to regular liposomes with gold coated nanoparticles. The interactions between liposomes (with thiolated and regular samples) and the gold coated magnetic nanoparticles show that the thiolated sample has a significant shift in transition temperature due to gold–thiol interaction over time. Interestingly, the liposomes examined in this work show a tendency to release more CF when the dilution media is distilled water instead of PBS. We have concluded that this behavior is due to the osmotic effect on liposomal stability under different dilution media. Distilled water makes the surroundings of liposomes more dilute than the liposomal core (which contains CF solution in PBS). The increase in release of CF before and after the addition of magnetic NPs shows that there is strong interaction of magnetic NPs with liposomes under the application of magnetic pulses. Though the bare iron oxide NPs only attach to the liposomes via physisorption, they can still disrupt the liposomal bilayer when magnetic pulses are applied. The gold coated iron oxide NP with thiolated liposome samples exhibit increased release of CF due to the strong binding of NPs onto the surfaces of the liposomes by gold–thiol bonds. The bonded NPs are nearer to the bare iron oxide NPs, and hence under magnetic pulses, they can rupture the lipid bilayer more efficiently, enhancing the release of CF. Furthermore, the liposomes under the influence of pulsed magnetic fields produce very efficient CF releases in a unit time compared literature values of previous work.

Supplementary Materials: The following are available online at <http://www.mdpi.com/2312-7481/6/4/52/s1>: Figure S1: (A) TEM image of synthesized iron oxide nanoparticles; (B) TEM image of gold coated synthesized iron oxide nanoparticles; (C) TEM image of gold coated commercial iron oxide nanoparticles. Figure S2: The EDX analysis of synthesized iron oxide nanoparticles. Figure S3: The EDX analysis of gold coated commercial iron oxide nanoparticles. Figure S4: Line scan map of gold coated commercial iron oxide nanoparticles. Figure S5: The EDX analysis of gold coated synthetic iron oxide nanoparticles. Figure S6: Line scan map of gold coated synthetic iron oxide nanoparticles. Figure S7: The images showing (A) gold coated commercial iron oxide nanoparticles (B) synthetic iron oxide nanoparticles, on liposomal surface providing the evidence of Au-SH chemisorption.

Figure S8. The size distribution of liposomes. Figure S9. The normalized release factor of CF from thiolated liposomes after the completion of Thermal cycle mentioned in Section 4.4. This shows the reproducibility of method of dyes encapsulation as well as CF release assay. Figure S10. The comparison of thermal profile for percentage CF release from different samples. (n = 6) showing reproducibility of the method used.

Author Contributions: Both authors equally contributed to the research presented in this manuscript. All authors have read and agree to the published version of the manuscript.

Funding: This research was funded by NSF #1608344 and Core Facility Equipment Awards from Terry Johnson Cancer Center.

Acknowledgments: The authors would like to acknowledge the support of NSF through grants NSF #1608344 and the Terry Johnson Cancer Center at KSU for funding the construction of the pulsed magnet.

Conflicts of Interest: The authors declare no conflict of interest.

References

1. Torchilin, V.P. Recent advances with liposomes as pharmaceutical carriers. *Nat. Rev. Drug Discov.* **2005**, *4*, 145–160. [[CrossRef](#)] [[PubMed](#)]
2. Woodle, M.C. Sterically stabilized liposome therapeutics. *Adv. Drug Del. Rev.* **1995**, *16*, 249–265. [[CrossRef](#)]
3. Charrois, G.J.R.; Allen, T.M. Rate of biodistribution of STEALTH liposomes to tumor and skin: Influence of liposome diameter and implications for toxicity and therapeutic activity. *Biochim. Biophys. Acta* **2003**, *1609*, 102–108. [[CrossRef](#)]
4. Nappini, S.; Bombelli, F.B.; Bonini, M.; Nordèn, B.; Baglioni, P. Magnetoliposomes for controlled drug release in the presence of low-frequency magnetic field. *Soft Matter* **2010**, *6*, 154–162. [[CrossRef](#)]
5. Al-Jamal, W.T.; Al-Jamal, K.T.; Bomans, P.H.; Frederik, P.M.; Kostarelos, K. Functionalized quantum-dot-liposome hybrids as multimodal nanoparticles for cancer. *Small* **2008**, *4*, 1406–1415. [[CrossRef](#)]
6. Nappini, S.; Bonini, M.; Bombelli, F.B.; Pineider, F.; Sangregorio, C.; Baglioni, P.; Norden, B. Controlled drug release under a low frequency magnetic field: Effect of the citrate coating on magnetoliposomes stability. *Soft Matter* **2011**, *7*, 1025–1037. [[CrossRef](#)]
7. Kloepper, J.A.; Cohen, N.; Nadeau, J.L. FRET Between CdSe Quantum Dots in lipid vesicles and Water- and Lipid- soluble dyes. *J. Phys. Chem. B* **2004**, *108*, 17042–17049. [[CrossRef](#)]
8. Nappini, S.; Bonini, M.; Ridi, F.; Baglioni, P. Structure and permeability of magnetoliposomes loaded with hydrophobic magnetic nanoparticles in the presence of a low frequency magnetic field. *Soft Matter* **2011**, *7*, 4801–4811. [[CrossRef](#)]
9. Needham, D.; Dewhirst, M.W. The development and testing of a new temperature-sensitive drug delivery system for the treatment of solid tumors. *Adv. Drug Delivery Rev.* **2001**, *53*, 285. [[CrossRef](#)]
10. Amstad, E.; Kohlbrecher, J.; Muller, E.; Schweizer, T.; Textor, M.; Reimhult, E. Triggered Release from Liposomes through Magnetic Actuation of Iron Oxide Nanoparticle Containing Membranes. *Nano Lett.* **2011**, *11*, 1664–1670. [[CrossRef](#)]
11. Masaharu, U.; Shoshin, Y.; Isamu, H. Characteristics of the Membrane Permeability of Temperature-Sensitive Liposome. *Bull. Chem. Soc. Jpn.* **1991**, *64*, 1588–1593. [[CrossRef](#)]
12. Ganta, S.; Devalapally, H.; Shahiwala, A.; Amiji, M. A review of stimuli-responsive nanocarriers for drug and gene delivery. *J. Control. Release* **2008**, *126*, 187–204. [[CrossRef](#)]
13. Hegh, D.Y.; Mackay, S.M.; Tan, E.W. Pulsatile release from pH triggered imidazoline switchable surfactant liposomes. *RSC Adv.* **2016**, *6*, 56859–56866. [[CrossRef](#)]
14. Wu, G.; Mikhailovsky, A.; Khant, H.A.; Fu, C.; Chiu, W.; Zasadzinski, J.A. Remotely Triggered Liposome Release by Near-Infrared Light Absorption via Hollow Gold Nanoshells. *J. Am. Chem. Soc.* **2008**, *130*, 8175–8177. [[CrossRef](#)]
15. Schroeder, A.; Kost, J.; Barenholz, Y. Ultrasound, liposomes, and drug delivery: Principles for using ultrasound to control the release of drugs from liposomes. *Chem. Phys. Lipids* **2009**, *162*, 1–16. [[CrossRef](#)]
16. Malekar, S.A.; Sarode, A.L.; Bach II, A.C.; Bose, A.; Bothun, G.; Worthen, D.R. Radio Frequency-Activated Nanoliposomes for Controlled Combination Drug Delivery. *AAPS PharmSciTech* **2015**, *16*, 1335–1343. [[CrossRef](#)]
17. Tai, L.A.; Tsai, P.J.; Wang, Y.C.; Wang, Y.J.; Lo, L.W.; Yang, C.S. Thermosensitive liposomes entrapping iron oxide nanoparticles for controllable drug release. *Nanotechnology* **2009**, *20*, 135101. [[CrossRef](#)]

18. Nardoni, M.; Valle, E.D.; Liberti, M.; Relucenti, M.; Casadei, M.A.; Paolicelli, P.; Apollonio, F.; Petralito, S. Can Pulsed Electromagnetic Fields Trigger On-Demand Drug Release from High-Tm Magnetoliposomes? *Nanomaterials* **2018**, *8*, 196. [[CrossRef](#)]
19. Shaghasemi, B.S.; Virk, M.M.; Reimhult, E. Optimization of Magneto-thermally Controlled Release Kinetics by Tuning of Magnetoliposome Composition and Structure. *Sci. Rep.* **2017**, *7*, 7474. [[CrossRef](#)]
20. Wong, D.W.; Gan, W.L.; Liu, N.; Lew, W.S. Magneto-actuated cell apoptosis by biaxial pulsed magnetic field. *Sci. Rep.* **2017**, *7*, 10919. [[CrossRef](#)]
21. Goya, G.F.; Grazu, V.; Ibarra, M.R. Magnetic Nanoparticles for Cancer Therapy. *Curr. Nanosci.* **2008**, *4*, 1–16. [[CrossRef](#)]
22. Pankhurst, Q.A.; Connolly, J.; Jones, S.K.; Dobson, J. Applications of magnetic nanoparticles in biomedicine. *J. Phys. D Appl. Phys.* **2003**, *36*, R167. [[CrossRef](#)]
23. Ahmed, S.E.; Moussa, H.G.; Martins, A.M.; Al-Sayah, M.H.; Hussein, G.A. Effect of pH, ultrasound frequency and power density on the release of calcein from stealth liposomes. *Eur. J. Nanomed.* **2016**, *8*, 31–43. [[CrossRef](#)]
24. Steinberg, Y.; Schroeder, A.; Talmon, Y.; Schmidt, J.; Khalfin, R.L.; Cohen, Y.; Devoisselle, J.-M.; Begu, S.; Avnir, D. Triggered Release of Aqueous Content from Liposome-Derived Sol-Gel Nanocapsules. *Langmuir* **2007**, *23*, 12024–12031. [[CrossRef](#)]
25. Jozefczak, A.; Kaczmarek, K.; Hornowski, T.; Kubovcikova, M.; Rozynek, Z.; Timko, M.; Skumeil, A. Magnetic nanoparticles for enhancing the effectiveness of ultrasonic hyperthermia. *Appl. Phys. Lett.* **2016**, *108*, 263701. [[CrossRef](#)]
26. Carrey, J.; Connord, V.; Respaud, M. Ultrasound generation and high-frequency motion of magnetic nanoparticles in an alternating magnetic field: Toward intracellular ultrasound therapy? *Appl. Phys. Lett.* **2013**, *102*, 232404. [[CrossRef](#)]
27. Mehrmohammadi, M.; Qu, M.; Ma, L.L.; Romanovicz, D.K.; Johnston, K.P.; Sokolov, K.V.; Emelianov, S.Y. Pulsed magneto-motive ultrasound imaging to detect intracellular trafficking of magnetic nanoparticles. *Nanotechnology* **2011**, *22*, 415105. [[CrossRef](#)]
28. Podaru, G.V.; Prakash, P.; Chikan, V. Magnetic Field Induced Ultrasound from Colloidal Superparamagnetic Nanoparticles. *J. Phys. Chem. C* **2016**, *120*, 2386–2391. [[CrossRef](#)]
29. Hu, G.; He, B. Magnetoacoustic Imaging of Magnetic Iron Oxide Nanoparticles Embedded in Biological Tissues with Microsecond Magnetic Stimulation. *Appl. Phys. Lett.* **2012**, *100*, 013704. [[CrossRef](#)] [[PubMed](#)]
30. Callen, E.; Callen, H.B. Magnetostriction Forced Magnetostriction and Anomalous Thermal Expansion in Ferromagnets. *Phys. Rev.* **1965**, *139*, A455. [[CrossRef](#)]
31. Podaru, G.; Ogden, S.; Baxter, A.; Shrestha, T.; Ren, S.; Thapa, P.; Dani, R.K.; Wang, H.; Basel, M.T.; Prakash, P.; et al. Pulsed Magnetic Field Induced Fast Drug Release from Magneto Liposomes Via Ultrasound Generation. *J. Phys. Chem. B* **2014**, *118*, 11715–11722. [[CrossRef](#)]
32. Love, J.C.; Estroff, L.A.; Kriebel, J.K.; Nuzzo, R.G.; Whitesides, G.M. Self-Assembled Monolayers of Thiolates on Metals as a Form of Nanotechnology. *Chem. Rev.* **2005**, *105*, 1103–1170. [[CrossRef](#)]
33. Nappini, S.; Fogli, S.; Castroflorio, B.; Bonini, M.; Bombelli, F.B.; Baglioni, P. Magnetic field responsive drug release from magnetoliposomes in biological fluids. *J. Mater. Chem. B* **2016**, *4*, 716–725. [[CrossRef](#)]
34. Das, M.; Dahal, U.; Mesele, O.; Liang, D.; Cui, Q. Molecular Dynamics Simulation of Interaction between Functionalized Nanoparticles with Lipid Membranes: Analysis of Coarse-Grained Models. *J. Phys. Chem. B* **2019**, *123*, 10547–10561. [[CrossRef](#)]
35. Chakraborty, S.; Abbasi, A.; Bothun, G.D.; Nagao, M.; Kitchens, C.L. Phospholipid Bilayer Softening Due to Hydrophobic Gold Nanoparticle Inclusions. *Langmuir* **2018**, *34*, 13416–13425. [[CrossRef](#)]
36. Häffner, S.M.; Malmsten, M. Membrane interactions and antimicrobial effects of inorganic nanoparticles. *Adv. Colloid Interface Sci.* **2017**, *248*, 105–128. [[CrossRef](#)]
37. Liburdy, R.P.; Tenforde, T.S.; Magin, R.L. Magnetic Field-Induced Drug Permeability in Liposome Vesicles. *Radiat. Res.* **1986**, *108*, 102–111. [[CrossRef](#)]
38. Liburdy, R.P.; Tenforde, T.S. Magnetic Deformation of Phospholipid Bilayers: Effects on Liposome Shape and Solute Permeability at Prephase Transition Temperatures. *J. Theor. Biol.* **1988**, *133*, 385–396. [[CrossRef](#)]
39. Liu, J.F.; Neel, N.; Dang, P.; Lamb, M.; McKenna, J.; Rodgers, L.; Litt, B.; Cheng, Z.; Tsourkas, A.; Issadore, D. Radiofrequency-Triggered Drug Release from Nanoliposomes with Millimeter-Scale Resolution Using a Superimposed Static Gating Field. *Small* **2018**, *14*, e1802563. [[CrossRef](#)]

40. Hulangamuwa, W.; Acharya, B.; Chikan, V.; Rafferty, R.J. Triggering Passive Molecular Transport into Cells with a Combination of Inhomogeneous Magnetic Fields and Magnetic Nanoparticles. *ACS Appl. Nano Mater.* **2020**, *3*, 2414–2420. [[CrossRef](#)]
41. Sharma, P.; Holliger, N.; Pfromm, P.H.; Liu, B.; Chikan, V. Size-Controlled Synthesis of Iron and Iron Oxide Nanoparticles by the Rapid Inductive Heating Method. *ACS Omega* **2020**, *5*, 19853–19860. [[CrossRef](#)]
42. Xu, Z.; Hou, Y.; Sun, S. Magnetic Core/Shell Fe₃O₄/Au and Fe₃O₄/Au/Ag Nanoparticles with Tunable Plasmonic Properties. *J. Am. Chem. Soc.* **2007**, *129*, 8698–8699. [[CrossRef](#)]
43. Lyon, J.L.; Fleming, D.A.; Stone, M.B.; Schiffer, P.; Williams, M.E. Synthesis of Fe Oxide Core/Au Shell Nanoparticles by Iterative Hydroxylamine Seeding. *Nano Lett.* **2004**, *4*, 719–723. [[CrossRef](#)]
44. Brown, K.R.; Walter, D.G.; Natan, M.J. Seeding of Colloidal Au Nanoparticle Solutions. 2. Improved Control of Particle Size and Shape. *Chem. Mater.* **2000**, *12*, 306–313. [[CrossRef](#)]

Publisher's Note: MDPI stays neutral with regard to jurisdictional claims in published maps and institutional affiliations.



© 2020 by the authors. Licensee MDPI, Basel, Switzerland. This article is an open access article distributed under the terms and conditions of the Creative Commons Attribution (CC BY) license (<http://creativecommons.org/licenses/by/4.0/>).